The H_2O molecule in the former complex is coordinated, but in the $A_2[UO_2(O_2)C_2O_4]\cdot H_2O$ case it is present as lattice water.

The complex species $[UO_2(O_2)SO_4(H_2O)]^{2-}$ very likely has a hexacoordinated polymeric structure through a –U–O–O–U–O–O–U– chain containing peroxide bridges. The complex $[UO_2(O_2)C_2O_4]^{2-}$ ion may be a hexacoordinated monomer; however, the possibility of a polymeric structure through a weak –U=O···U=O··· interaction cannot be totally ruled out.

Acknowledgment. Financial support from the Department of Atomic Energy is gratefully acknowledged. The authors thank the CSIR, New Delhi, for awarding fellowships to M.B. and R.N.D.P. and Professor A. L. Verma of the Department of Physics for extending his laser Raman facilities.

Registry No. $(NH_4)_2[UO_2(O_2)SO_4(H_2O)]$, 102149-54-2; $Na_2[UO_2(O_2)SO_4(H_2O)]$, 102149-56-4; $(NH_4)_2[UO_2(O_2)C_2O_4]$, 94535-39-4; $Na_2[UO_2(O_2)C_2O_4]$, 102149-57-5; $K_2[UO_2(O_2)C_2O_4]$, 102149-58-6.

Contribution from the Department of Chemistry, The University of North Carolina, Chapel Hill, North Carolina 27514

Redox and Spectral Properties of the Cis and Trans Isomers of the Osmium(VI) Dioxo Complex $[(bpy)_2Os(O)_2](ClO_4)_2$

John C. Dobson, Kenneth J. Takeuchi, David W. Pipes, Daniel A. Geselowitz, and Thomas J. Meyer*

Received February 20, 1986

The cis and trans isomers of $[(bpy)_2Os(O)_2](ClO_4)_2$ (bpy = 2,2′-bipyridine) have been prepared and characterized and their redox properties in aqueous solution investigated by using electrochemical techniques. Plots of $E_{1/2}$ vs. pH for a series of redox couples that appear involving oxidation states II–VI are revealing both in terms of the relative stabilities of the various oxidation states for each isomer and in terms of the relative stabilities of the cis and trans isomers in different oxidation states. The cis isomer undergoes bpy ligand loss in aqueous solution on a time scale of minutes by chelate ring opening followed by ligand loss. Upon reduction to Os(III) or Os(II) the trans isomer is unstable with respect to isomerization to the cis isomer. Comparisons of the redox properties of the isomeric pair give insight into the factors that dictate the relative stabilities of oxidation states and suggest possibilities for the control of the redox potentials, which play a key role in the ability of polypyridyl oxo complexes of ruthenium and osmium to act as redox catalysts.

Introduction

In recent work we have shown that access to a series of metal oxo complexes of Ru and Os is possible based on oxidation of the corresponding aqua complexes, e.g., reaction 1 (b = bpy, 2,2′-bipyridine).[1] In most accessible pH domains, the oxidation process

$$[b_2(py)Ru^{II}\text{–}OH_2]^{2+} \xrightarrow{-e^-,\,-H^+} [b_2(py)Ru^{III}\text{–}OH]^{2+} \xrightarrow{-e^-,\,H^+} [b_2(py)Ru^{IV}{=}O]^{2+} \quad (1)$$

is accompanied by proton loss and stabilization of higher oxidation states by electronic donation from bound hydroxo or oxo groups. Synthetically, this approach to the preparation of metal oxo complexes has the advantage of starting with the synthetically accessible lower oxidation states to give higher oxidation states that are frequently good stoichiometric or even catalytic oxidants.

In a preliminary communication we noted an extensive redox chemistry of this kind based on $[(bpy)_2M(OH_2)_2]^{2+}$ (M = Ru or Os) which extended from oxidation states II through VI.[1c] In this paper we elaborate on the Os chemistry and note the existence of cis and trans isomers of $[(bpy)_2Os^{VI}(O)_2]^{2+}$. The cis isomer appears to be the first example of a d^2 *cis*-dioxo complex.

Experimental Section

Materials. Burdick and Jackson spectrograde acetonitrile was distilled under argon over P_2O_5 on a Vigreaux column. Ce(IV) perchlorate in perchloric acid solution (0.5 N) was purchased from G. F. Smith Chemical Co. Buffer solutions for electrochemical and spectroscopic measurements were prepared from $HClO_4$ acid solutions with $LiClO_4$ added as additional electrolyte (pH 0–2) and mono-, di-, and tribasic phosphate (pH 3–12) to maintain a minimum ionic strength of 0.1 M. The pH measurements were made with a radiometer pHM62 pH meter. All other materials were obtained as reagent grade and used without further purification.

Elemental Analysis. Microanalyses were conducted by Galbraith Laboratories, Knoxville, TN.

Preparations. The syntheses of $(bpy)_2OsCO_3$ and $(phen)Os(O)_2(OH)_2$ have been described previously.[2,3]

***cis*-$[(bpy)_2Os(O)_2](ClO_4)_2$.** To 10 mL of 2 M $HClO_4$ was added 50 mg (0.089 mmol) of bpy_2OsCO_3. The resulting solution was degassed with argon for 15 min and then filtered through a medium glass frit. To the stirred filtrate was added 1 mL of 0.5 N cerium(IV) perchlorate in perchloric acid solution. The green microcrystalline precipitate was filtered off, washed with 3 × 3 mL portions of ether, and then dried in vacuo. Yield: 34 mg, 52%. Anal. Calcd for $OsC_{10}H_{16}O_{10}Cl_2$: C, 32.71; H, 2.18; N, 7.63; Cl, 9.68. Found: C, 32.57; H, 2.35; N, 7.39; Cl, 9.58.

***trans*-$[(bpy)_2Os(O)_2](ClO_4)_2$.** To 20 mL of rigorously dry acetonitrile was added 50 mg (0.068 mmol) of *cis*-$[(bpy)_2Os(O)_2](ClO_4)_2$. The solution was heated at gentle reflux for 20 min with magnetic stirring under an inert argon atmosphere. After this time the solution was allowed to cool to room temperature and the resulting precipitate filtered onto a medium glass frit. Dry conditions are essential as bipyridine loss from *cis*-$[(bpy)_2Os(O)_2]^{2+}$ and subsequent dimer formation upon heating to yield the dioxo-bridged dimer $[(bpy)(O)_2Os]_2O_2^{4+}$ is competitive with isomerization. The beige solid was washed with 1 mL of ether and dried in vacuo. Yield: 24 mg, 48%. Anal. Calcd for $OsC_{10}H_{16}O_{10}Cl_2$: C, 32.71; H, 2.18; N, 7.63; Cl, 9.68. Found: C, 32.83; H, 2.18; N, 7.65; Cl, 9.46.

Measurements. Aqueous solutions of *cis*-$[(bpy)_2Os(OH_2)_2]^{2+}$ were prepared by dissolving the appropriate amount of $(bpy)_2OsCO_3$ in acidic solution. The diaqua complex is formed by protonation and loss of carbonate as CO_2

$$(bpy)_2Os(CO_3) + 2H^+ + H_2O \rightarrow [(bpy)_2Os(OH_2)_2]^{2+} + CO_2$$

Spectroscopy. Routine UV–vis spectra were recorded in quartz cells at room temperature on a Bausch and Lomb Model 210 spectrophotometer. Proton NMR spectra were recorded on a Bruker 250-MHz Fourier transform spectrometer and referenced to either Me_4Si or DSS accordingly. Spectra were recorded within $^1/_2$ h of sample preparation. IR measurements were obtained as KBr pellets or Nujol mulls on a Nicolet Model 20 DX FTIR.

(1) (a) Moyer, B. A.; Meyer, T. J. *Inorg. Chem.* **1981**, *20*, 436. (b) Takeuchi, K. J.; Thompson, M. S.; Pipes, D. W.; Meyer, T. J. *Inorg. Chem.* **1984**, *23*, 1845. (c) Takeuchi, K. J.; Samuels, G. J.; Gersten, S. W.; Gilbert, J. A.; Meyer, T. J. *Inorg. Chem.* **1983**, *22*, 1407.

(2) (a) Kober, E. M. Ph.D. Thesis, University of North Carolina at Chapel Hill, 1981. (b) Kober, E. M.; Casper, J. V.; Sullivan, B. P.; Meyer, T. J., manuscript in preparation.

(3) Chang, C. H.; Midden, W. R.; Deetz, J. S.; Behrman, E. J. *Inorg. Chem.* **1979**, *18*, 1364.

(4) (a) Ray, M. M.; Sarkar, A. K. *Sci. Cult.* **1966**, *32*(12), 593. (b) Nikol'ski, A. B.; D'Yachenko, Yu. I.; Myund, L. A. *Russ. J. Inorg. Chem.* (*Engl. Transl.*) **1974**, *19*(9), 1368.

0020-1669/86/1325-2357$01.50/0

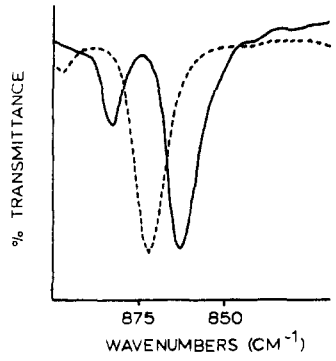

Figure 1. IR absorption spectra (Nujol mull) of *cis*- (solid line) and *trans*- (dashed line) $[(bpy)_2Os(O)_2](ClO_4)_2$ in the region 820–900 cm^{-1}.

Electrochemistry. Electrochemical measurements were made by using a PAR Model 173 potentiostat control with a PAR Model 175 universal programmer as a sweep generator for voltammetry experiments. Measurements were made vs. the saturated sodium chloride calomel electrode (SSCE) or saturated potassium chloride calomel electrode (SCE) at 25 ± 2 °C and are uncorrected for junction potential effects. Cyclic voltammetry measurements were performed in a 10-mL beaker with either a 2-cm^2 glassy-carbon-disk electrode (Tokai Carbon, Inc.) or a carbon-paste electrode as the working electrode and a platinum wire as the auxiliary electrode. Coulometry experiments were performed in three-compartment cells with a platinum-screen electrode. Double-potential-step chronoamperometry was performed with a glassy-carbon electrode in a three-compartment cell. The potentiostat was driven by a computer system consisting of an IBM PC, a DT2801 A/D board (DATA Translation, Inc.), and a program written on the ASYST system (MacMillam Software, Inc.). Rotating-disk experiments were performed in a three-compartment cell by using a glassy-carbon RDE with a rotation rate of 1600 rpm. Differential pulse voltammetry was performed with a PAR 174 electrochemical analyzer using a carbon-paste working electrode. The sweep rate was 2 mV/s, and the peak amplitude was 5 mV.

Kinetic Measurements. The loss of bipyridine from *cis*-$[(bpy)_2Os(O)_2]^{2+}$ in aqueous solution was monitored spectrophotometrically. Concentrated solutions of *cis*-$[(bpy)_2Os(O)_2]^{2+}$ in dry CH_3CN (in which the complex is stable) were injected into an excess volume of 0.1 M phosphate buffer solutions. The absorbance changes were monitored at λ = 283 nm for pH >4.4 and at λ = 302 nm for pH <4.4, which correspond to λ_{max} values for free bipyridine. Measurements were made on a Hewlett-Packard Model 8450A UV–vis diode-array spectrophotometer. First-order rate constants, k, were calculated on the basis of a least-squares fit (uniform weighting) to the relation $\ln|A_\infty - A_t| = -kt + \ln|A_\infty - A_0|$ where A_∞ and A_0 are the final and initial absorbances, respectively, and A_t is the absorbance measured at time t. Data were collected over several half-lives. A_∞ was adjusted over a small range to give maximum correlation coefficients.

Results

Spectra. The IR spectra of the *cis*- and *trans*-$[(bpy)_2Os(O)_2]^{2+}$ complexes are shown in Figure 1. The cis complex shows two peaks in the ν(Os=O) region at 883 and 863 cm^{-1}, which can be assigned to the symmetric and asymmetric Os=O stretches, respectively, and are indicative of the *cis*-dioxo structure. The trans complex shows a single peak in this region at 872 cm^{-1}, as expected.[5] The ^1H NMR spectra of *cis*-$[(bpy)_2Os(O)_2]^{2+}$ in CD_3CN and of *trans*-$[(bpy)_2Os(O)_2]^{2+}$ in Me_2SO-d_6 are shown in Figure 2. The cis complex is both soluble and stable in dry CH_3CN while the trans complex is sparingly soluble in CH_3CN, necessitating the use of Me_2SO-d_6 as the NMR solvent. The spectrum of the cis complex is consistent with the presence of resonances for eight nonequivalent protons while that of the trans isomer shows resonances for four nonequivalent protons. The change in the pattern of resonances is consistent with the change from C_2 to D_{2h} symmetry upon isomerization from the cis to the trans isomers.[6]

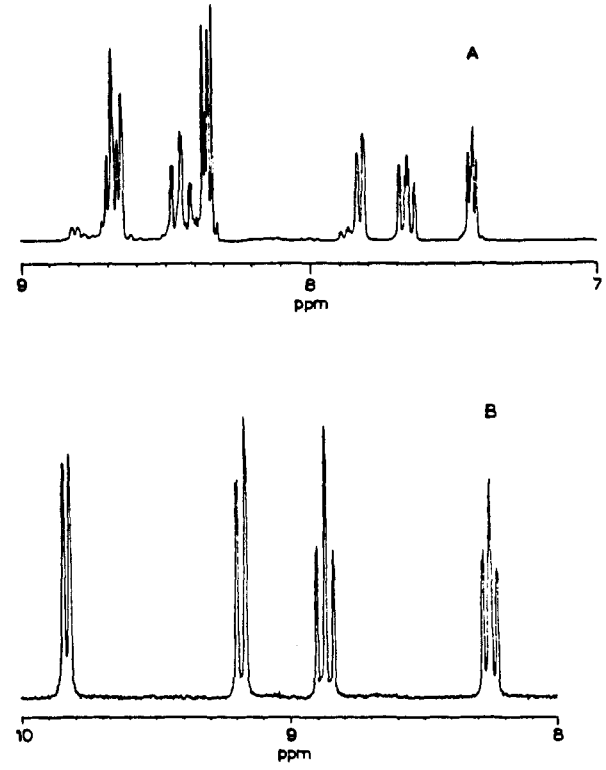

Figure 2. ^1H NMR of (a) *cis*-$[(bpy)_2Os(O)_2](ClO_4)_2$ in CD_3CN and (b) *trans*-$[(bpy)_2Os(O)_2](ClO_4)_2$ in Me_2SO-d_6.

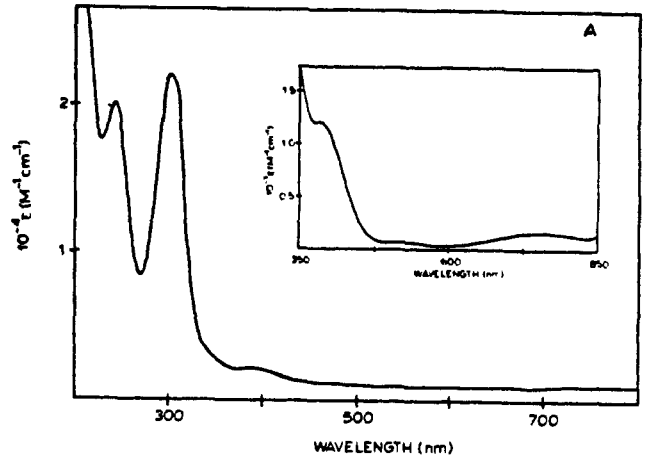

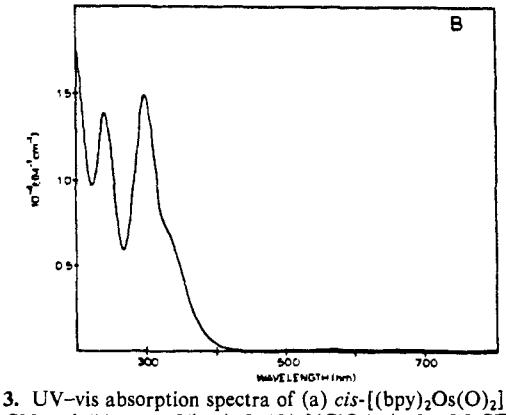

Figure 3. UV–vis absorption spectra of (a) *cis*-$[(bpy)_2Os(O)_2](ClO_4)_2$ in CH_3CN and (b) *trans*-$[(bpy)_2Os(O)_2](ClO_4)_2$ in 0.1 M CF_3SO_3H.

The UV–vis spectra of *cis*-$[(bpy)_2Os(O)_2]^{2+}$ in CH_3CN and of *trans*-$[(bpy)_2Os(O)_2]^{2+}$ in 0.1 M aqueous CF_3SO_3H are dominated by two high-energy peaks arising from $\pi \rightarrow \pi^*$ (bpy) transitions. In the spectra shown in Figure 3 peaks appear at 303

(5) (a) Collins, R. J.; Jones, J.; Griffith, W. P. *J. Chem. Soc., Dalton Trans.* **1974**, 1094. (b) Jezowska-Trebiatowska, B.; Hanuza, J.; Baluka, M. *Acta Phys. Pol., A* **1970**, *A38*, 563.
(6) Walsh, J. L.; Durham, B. *Inorg. Chem.* **1982**, *21*, 329.

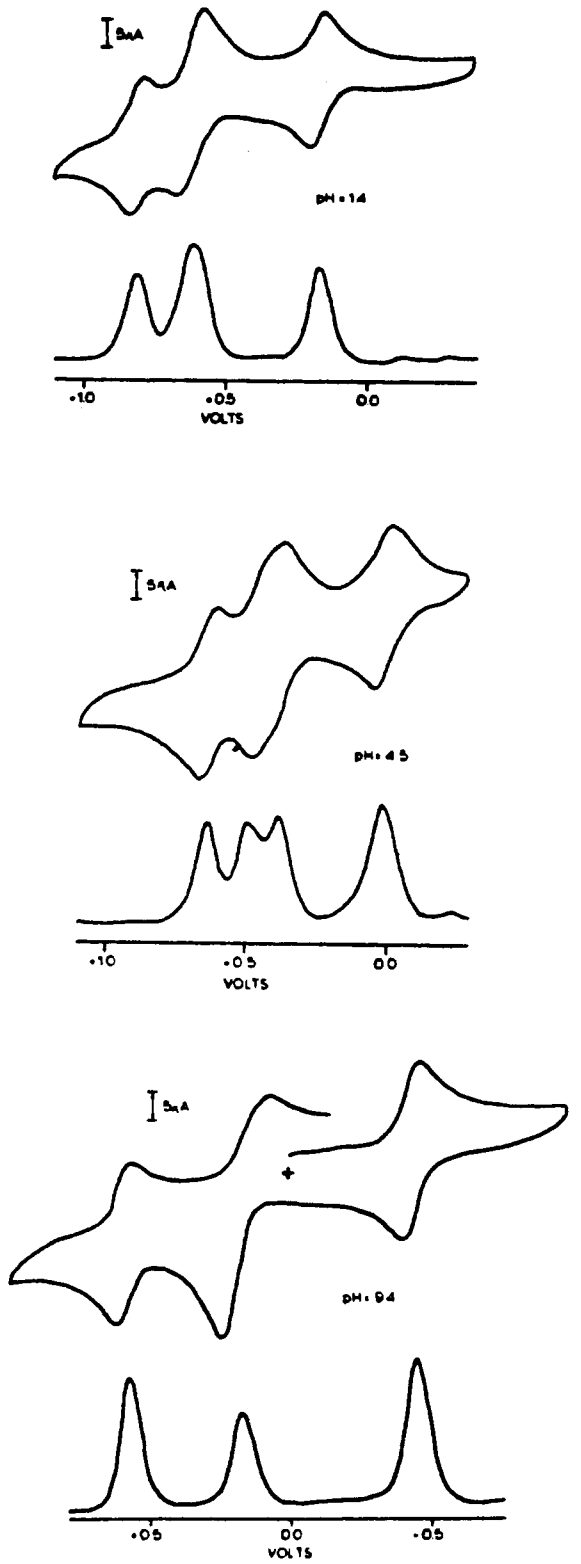

Figure 4. Cyclic voltammograms (100 mV/s) and differential pulse polargrams (2 mV/s) of ~2 mM *cis*-$[(bpy)_2Os(OH_2)_2]^{2+}$ (μ = 0.1 M; vs. SSCE) at different pH values.

nm (ϵ ~22000) and 243 nm (ϵ ~20000) for the cis complex in CH_3CN and at 301 nm (ϵ ~15000) and 225 nm (ϵ ~14000) for the trans complex in 0.1 M CF_3SO_3H. The cis complex also has absorption bands at λ_{max} = 390 nm (ϵ ~1200), 525 nm (ϵ ~75), and 750 nm (ϵ ~250). The only additional feature in the spectrum of the trans complex is a distinctive shoulder present on the band at 301 nm.

Electrochemistry. Electrochemical experiments were performed on solutions of *cis*-$[(bpy)_2Os(OH_2)_2]^{2+}$ because of the instability of aqueous solutions of *cis*-$[(bpy)_2Os(O)_2]^{2+}$. The higher oxidation states are accessible by a series of sequential oxidations of the diaquo complex and are reversible on the time scale of the cyclic voltammetry experiments.

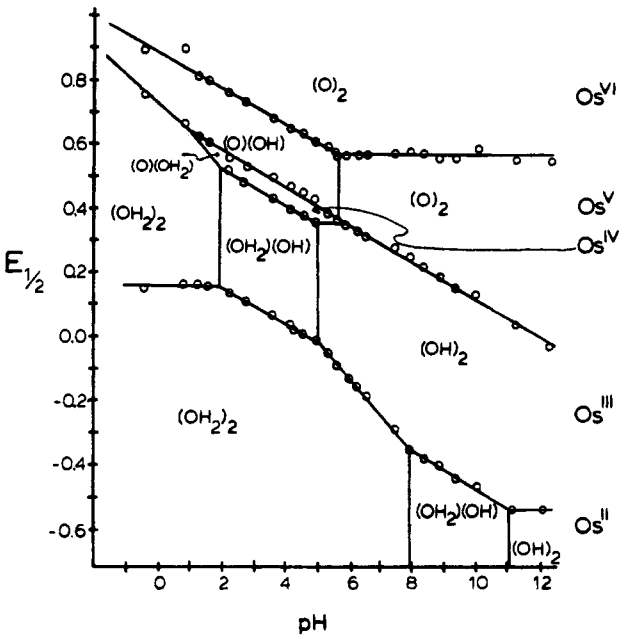

Figure 5. $E_{1/2}$ vs. pH (Pourbaix) diagram for *cis*-$[(bpy)_2Os(O)_2]^{2+}$. The pH–potential regions of stability for the various oxidation states of the complex are labeled as Os^{II}, Os^{III}, etc. The proton compositions of the various oxidation state forms are indicated, for example, by $(OH_2)_2$–Os^{II} for *cis*-$[(bpy)_2Os^{II}(OH_2)_2]^{2+}$. The lines through the experimental points represent $E_{1/2}$ values for the couple indicated. Vertical lines are drawn from the breaks in the $E_{1/2}$ lines and represent approximate pK_a values.

Representative cyclic voltammograms and differential pulse polarograms for solutions of *cis*-$[(bpy)_2Os(OH_2)_2]^{2+}$ at various pH values are presented in Figure 4. At pH 1.4, the first step, a one-electron process (n = 0.9 ± 0.1 by coulometry), at $E_{1/2}$ = 0.16 V is assigned to the Os(III)/Os(II) couple. It is followed by a two-electron step (inferred from relative peak areas) at $E_{1/2}$ = 0.61 V, which corresponds to the Os(V)/Os(III) couple, and finally by another one-electron step at $E_{1/2}$ = 0.81 V, attributable to the Os(VI)/Os(V) couple. Coulometric oxidation of *cis*-$[(bpy)_2Os^{III}(OH_2)_2]^{3+}$ at 1.0 V vs. SCE gave n = 2.9 ± 0.2, consistent with the pattern of a two-electron followed by a one-electron couple past Os(III). At pH 4.0, the Os(V)/Os(III) couple separates into two resolvable one-electron waves, providing evidence for both the Os(IV)/Os(III) and the Os(V)/Os(IV) couples.

The pH dependences of the reduction potentials for the various couples are summarized in a Pourbaix diagram[7] in Figure 5. In the diagram the oxidation state at the metal is indicated as is the complex's proton composition. For example, the abbreviation for $[Os^{III}(bpy)_2(OH)_2]^{2+}$ is $(OH)_2$–Os^{III}. The labeled areas indicate the potential–pH regions where the oxidation state with the proton content indicated is the dominant form. The lines show how the potentials of the various couples vary with pH. The pK_a values, estimated from the breaks in the $E_{1/2}$–pH lines, are shown as vertical lines on the Pourbaix diagram and pertain to the lower oxidation state of the two that constitute the couple.

Data points on the diagram were obtained from cyclic voltammetric $E_{1/2}$ values and lines drawn with slopes of either 0, −30, −59 or −88, or −118 mV/pH unit. The various slopes correspond to proton to electron ratios of 0, 0.5, 1.0 and 1.5, and 2.0, respectively, as calculated from the Nernst equation. Notice that in the pH range ~2–5, $E_{1/2}$ values for all four couples decrease linearly with increasing pH (slope −59 mV/pH unit), consistent with one-electron, one-proton couples in all cases. At pH <2 the Os(V)/Os(III) couple appears at the expense of the Os(V)/Os(IV)

(7) Douglas, B.; McDaniel, D. H.; Alexander, J. J. *Concepts and Models of Inorganic Chemistry*; Wiley: New York, 1983.

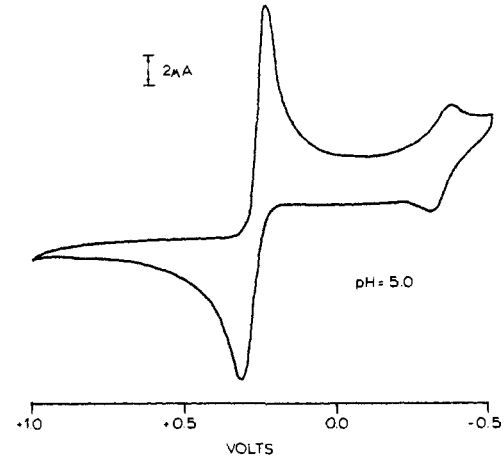

Figure 6. Cyclic voltammogram of ~2 mM *trans*-$[(bpy)_2Os(O)_2](ClO_4)_2$. Conditions: 20 mV/s; pH 5.0; μ = 0.1 M; vs. SCE.

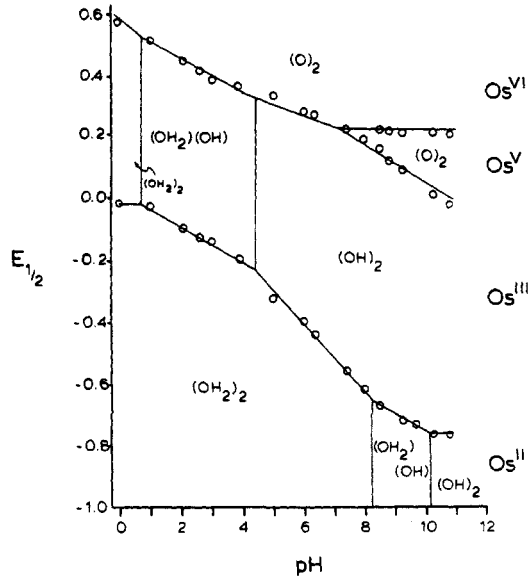

Figure 7. $E_{1/2}$ vs. pH (Pourbaix) diagram for *trans*-$[(bpy)_2Os(O)_2]^{2+}$. The data display uses the same format as described in Figure 5.

and Os(IV)/Os(III) couples. Its $E_{1/2}$ value increases linearly with decreasing pH (slope −88 mV/pH unit), which is consistent with a couple involving three protons and two electrons. At pH >5 the Os(V)/Os(III) couple again appears with a slope of −59 mV/pH unit, consistent with a two-electron two-proton couple. Above pH 7, the wave for the Os(V)/Os(III) couple becomes less reversible as shown by the increase in the peak-to-peak splitting (ΔE_p), as can be seen in the cyclic voltammogram in Figure 4 at pH 9.4.

Cyclic voltammetry experiments show a related chemistry for *trans*-$[(bpy)_2Os(O)_2]^{2+}$. Figure 6 shows the cyclic voltammogram for the trans complex at pH 5.0 and a scan rate of 20 mV/s. A one-electron process appears for the Os(III)/Os(II) couple at $E_{1/2}$ = −0.20 V vs. SCE along with a quasi-reversible, three-electron process at $E_{1/2}$ = 0.36 V for the Os(VI)/Os(III) couple. A rotating-disk voltammetry experiment verified a one to three ratio of currents for the assigned couples. The most notable feature of the pH-dependent studies appears near pH 8, where the three-electron wave splits into two waves, a pH-independent one-electron wave for the Os(VI)/Os(V) couple and a $2e^-/2H^+$ wave for the Os(V)/Os(III) couple.

A Pourbaix diagram for the trans couples is shown in Figure 7, where the $E_{1/2}$–pH lines were drawn with slopes depending on the electron–proton contents of the couples as follows: 0 mV/pH unit, $1e^-$; 39 mV/pH unit, $3e^-/2H^+$; 59 mV/pH unit, $1e^-/1H^+$ or $3e^-/3H^+$; 79 mV/pH unit, $3e^-/4H^+$; 118 mV/pH unit, $1e^-/2H^+$.

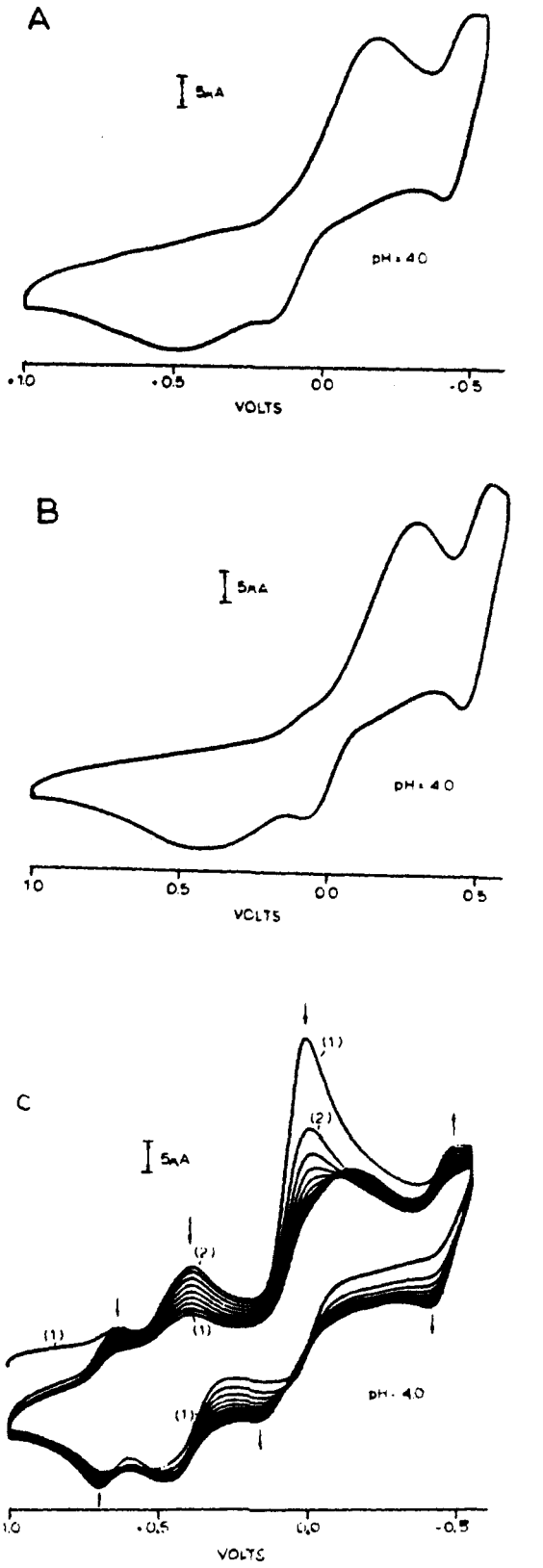

Figure 8. Cyclic voltammograms (vs. SCE) of (a) decomposition product of *cis*-$[(bpy)_2Os(O)_2]^{2+}$ and (b) $(phen)Os(O)_2(OH_2)$ (μ = 0.1 M; pH 4.0; scan rate 100 mV/s; concentration ~2 mM). Part c shows continuous-scan cyclic voltammograms of *cis*-$[(bpy)_2Os(O)_2]^{2+}$ at pH 4.0. The first scan was initiated at 1.0 V. The first two cycles are labeled. Arrows illustrate the direction of change of the peaks on subsequent scans.

Ligand Loss. In aqueous solution, *cis*-$[(bpy)_2Os(O)_2]^{2+}$ is unstable as shown by both electrochemical and spectrophotometric studies. The similarity of the cyclic voltammogram of the decomposition product of *cis*-$[(bpy)_2Os(O)_2]^{2+}$ (taken at pH 4.0 after several minutes) to the cyclic voltammogram of the known

(phen)Os(O)$_2$(OH)$_2$ complex as illustrated in Figure 8a,b suggests that the overall process involves the loss of a bipyridine ligand to form (bpy)Os(O)$_2$(OH)$_2$.

$$[(bpy)_2Os^{VI}(O)_2]^{2+} + 2H_2O \rightarrow (bpy)Os(O)_2(OH)_2 + bpy + 2H^+$$

Bipyridine loss from *cis*-[(bpy)$_2$Os(O)$_2$]$^{2+}$ was further supported by ^{1}H NMR studies. The spectrum of *cis*-[(bpy)$_2$Os(O)$_2$]$^{2+}$ in D$_2$O following decomposition shows four sharp resonances centered at 9.18, 8.60, 8.45, and 7.93 ppm (integration 1:1:1:1), which are consistent with a mono(bipyridine) osmium complex, while three broad resonances centered at 8.68, 8.28, and 7.73 ppm (integration 1:2:1) arise from free bipyridine in D$_2$O.

Further information concerning the mechanism of ligand loss can be deduced from the continuous-scan cyclic voltammogram shown in Figure 8c. The cyclic voltammogram was started at +1.0 V vs. SCE with a scan rate of 100 mV/s. The first scan was taken at time $t \sim 20$ s after addition of the solid sample to the solution. When the reaction was scanned negatively from 1.0 V, the first scan (1) showed small reductive waves at $E_p = 0.63$ and 0.38 V and a large reductive wave at $E_p = -0.03$ V. Upon reversal of scan direction a broad oxidative wave was observed at $E_p = 0.15$ V along with an apparent double peak at $\sim E_p = 0.5$ V and another single oxidative peak at $E_p = 0.71$ V. On the second scan (2) the reductive peaks at $E_p = 0.63$ and 0.38 V had grown and the peak at $E_p = -0.03$ V had decreased considerably. On subsequent scans the reductive peaks at $E_p = 0.63$, 0.38, and −0.03 V diminished while new reductive peaks appeared at $E_p = -0.16$ and −0.47 V. The oxidative peak at $E_p = 0.71$ V also diminished on subsequent scans while the broad peak at 0.15 V grew in and a new oxidative peak appeared at $E_p = -0.41$ V. The arrows in Figure 8c illustrate the direction of change of the peaks on subsequent scans. Eventually, the cyclic voltammogram becomes that shown in Figure 8a.

We interpret the data as follows: The initially added *cis*-[(bpy)$_2$Os(O)$_2$]$^{2+}$ is no longer present to an appreciable extent at the time of the first scan. The overall reaction to give (bpy)Os(O)$_2$(OH)$_2$ occurs on a time scale of several minutes. Apparently, the added *cis*-[(bpy)$_2$Os(O)$_2$]$^{2+}$ has already undergone a reaction to form an intermediate by the time the first scan was initiated. Upon reduction at potentials more negative than −0.03 V, the intermediate is apparently converted into *cis*-[(bpy)$_2$Os(OH$_2$)$_2$]$^{2+}$, as evidenced by the reappearance of the couple at $E_{1/2} = 0.68$ V (indicative of the Os(VI)/Os(V) couple) and the double peak (indicative of the Os(IV)/Os(III), Os(V)/Os(IV), and Os(IV)/Os(III) couples) at $\sim E_{1/2} = 0.44$ V. The overall kinetic scheme is

$$cis\text{-}[(bpy)_2Os(O)_2]^{2+} \xrightarrow{k_1} I \quad (2)$$

$$I \xrightarrow{k_2} (bpy)Os(O)_2(OH)_2 + bpy + 2H^+ \quad (3)$$

$$I \xrightarrow[<-0.03\ V]{\text{reduce}} cis\text{-}[(bpy)_2Os(OH_2)_2]^{2+} \quad (4)$$

Processes 2 and 3 comprise the reaction scheme that leads to decomposition while reaction 4 is an electrochemical reaction of the intermediate. As discussed later, the intermediate appears to contain a singly bound bpy ligand and process 4 is a chelate ring reclosure step following reduction to Os(II).

Kinetics data for the processes represented by k_1 and k_2 were obtained by repetitive-scan spectrophotometric studies. Representative UV–vis repetitive scans of *cis*-[(bpy)$_2$Os(O)$_2$]$^{2+}$ in aqueous solution taken at time intervals of every 2 s and every 30 s are presented in Figure 9a,b. The first process is more rapid and is the process followed in Figure 9a. The absorbance at $\lambda_{max} = 302$ nm decreases with each successive scan resulting in the buildup of intermediate I with a first-order rate constant, k_1, of 0.11 s^{-1} at room temperature (pH 6.0). The time dependence of the second process is shown in Figure 9b. The first reaction is essentially complete after the second scan in Figure 9b (30 s). A feature of note in the slower scans is the increase in absorbance

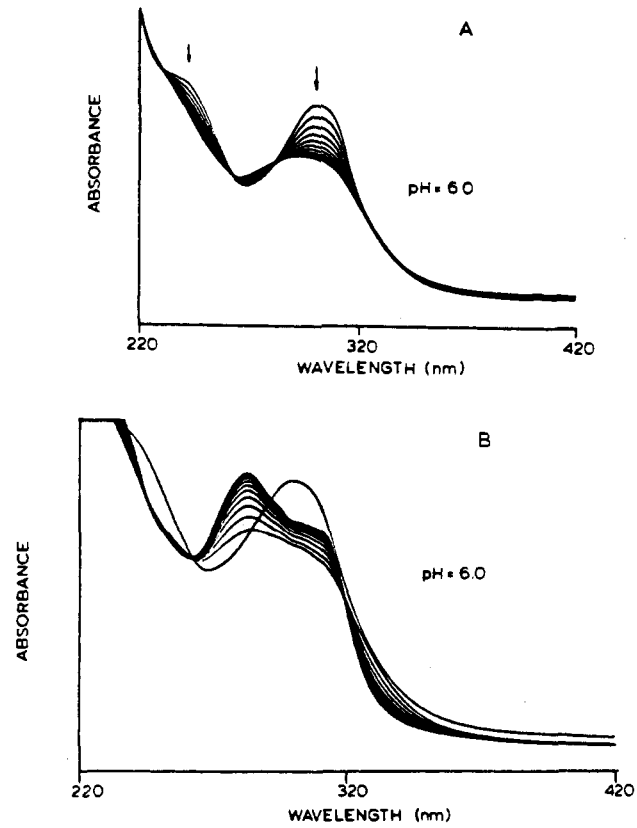

Figure 9. Spectral changes with time in the decomposition of $\sim 10^{-5}$ M *cis*-[(bpy)$_2$Os(O)$_2$]$^{2+}$. Scans were taken at room temperature in time intervals of (a) every 2 s for a total of 20 s and (b) every 30 s for a total of 300 s.

Table I. Rate Constant Data at 25 °C for Stepwise Decomposition of *cis*-[(bpy)$_2$Os(O)$_2$]$^{2+}$ in Aqueous Solution ($\mu = 0.1$ M)[a]

pH	10^3k_1, s^{-1}	10^3k_2, s^{-1}	pH	10^3k_1, s^{-1}	10^3k_2, s^{-1}
1.0	~50	≫50	5.0	109	7.8
2.0	~50	≫50	6.0	104	8.4
2.6	~70	≫70	7.0	145	10.2
3.0	~100	~20	8.0	151	13.2
4.0	~110	~10.9	9.0	190	13.2

[a] Note the scheme in reactions 2 and 3.

at $\lambda_{max} = 283$ nm, indicative of the formation of free bipyridine. For the slower process, $k_2 = 0.011$ s^{-1} (pH 6.0). At pH values of 4 and below, the free ligand exists as the bipyridinium ion ($pK_a = 4.3$) and λ_{max} shifts to 302 nm, which was used as a monitoring wavelength for both k_1 and k_2. Rate constant data as a function of pH are summarized in Table I. Repetition of selected runs demonstrates a reproducibility of ±5%.

In acidic solutions, at pH 1 or 2, there is no evidence for the buildup of an intermediate. Rather, *cis*-[(bpy)$_2$Os(O)$_2$]$^{2+}$ appears in a first-order process to give the bpy-loss product. From the data in Table I, k_1 is relatively insensitive to pH as is k_2 from pH 4 to 9. However, below pH 4, k_2 increases rapidly with decreasing pH. From our observations, by pH 2, the k_2 path is more rapid than the k_1 path and the concentration of the intermediate never reaches an appreciable level during the course of the reaction.

A double-potential-step chronoamperometric experiment was performed to confirm the kinetic data obtained spectrophotometrically. In the experiment a solution of *cis*-[(bpy)$_2$Os(OH$_2$)$_2$]$^{2+}$ was bulk electrolyzed to generate *cis*-[(bpy)$_2$Os^{III}(OH)$_2$]$^+$ at pH 6.0 so that a potential step could be applied in a potential region where the product, (bpy)Os(O)$_2$(OH)$_2$, is not electroactive. Following bulk electrolysis, an initial potential of 0.1 V was applied, followed by a potential step to 0.8 V and a following return step to a final potential of 0.1 V. The data were collected over several values of τ, the time difference between the first and second potential steps, and fit to the working curves described by Schwarz

and Shain.[8] The chronoamperometric data corroborated the presence of an EC mechanism.

Isomerization. When heated at reflux in dry CH_3CN, solutions containing *cis*-$[(bpy)_2Os(O)_2](ClO_4)_2$ give a beige precipitate. The precipitate is *trans*-$[(bpy)_2Os(O)_2](ClO_4)_2$. Attempts to synthesize *trans*-$[(bpy)_2Os(OH_2)_2]^{2+}$ by bulk electrolysis of *trans*-$[(bpy)_2Os(O)_2]^{2+}$ at 0.3 V and at pH 1 led to isomerization to *cis*-$[(bpy)_2Os(OH_2)_2]^{2+}$.

Discussion

***cis*- and *trans*-$[Os(bpy)_2(O)_2]^{2+}$.** Synthetically, *cis*- and *trans*-dioxo complexes are derived from *cis*-$(bpy)_2OsCO_3$. Acidification of the carbonato complex results in the formation of *cis*-$[(bpy)_2Os(OH_2)_2]^{2+}$, which was oxidized by Ce(IV) in acidic solution.

$$[(bpy)_2Os(OH_2)_2]^{2+} + 4Ce(IV) \rightarrow [(bpy)_2Os(O)_2]^{2+} + 4H^+ + 4Ce(III)$$

In the oxidative step it is crucial that rapid precipitation occurs because of the instability of the cis complex in aqueous solutions. The *cis*-$[(bpy)_2Os(O)_2]^{2+}$ complex is stable in dry CH_3CN at room temperature, but upon heating at reflux it undergoes isomerization to *trans*-$[(bpy)_2Os(O)_2]^{2+}$.

The characterization of the *cis*- and *trans*-$[(bpy)_2Os(O)_2]^{2+}$ complexes was based on elemental analysis, the parent ion peak in the previously reported mass spectrum of *cis*-$[(bpy)_2Os(O)_2]^{2+}$,[9] and IR and NMR data. The stereochemistry at *cis*-$[(bpy)_2Os(O)_2]^{2+}$ is shown by the presence of two (Os=O) stretches in the IR spectrum and by the presence of eight nonequivalent protons (the *cis*-bipyridine protons) in the ^1H NMR spectrum. Likewise, *trans*-$[(bpy)_2Os(O)_2]^{2+}$ has a single ν(Os=O) stretch in the IR spectrum and four nonequivalent protons in the ^1H NMR spectrum.

The absence of any sign of paramagnetic shifts in the ^1H NMR spectra of both *cis*- and *trans*-$[(bpy)_2Os(O)_2]^{2+}$ suggest a diamagnetic ground state for both. Diamagnetism is expected for the D_{2h} symmetry of the trans complex on the basis of the splitting of the dπ orbitals into d_{xz},d_{yz} and d_{xy} sets with the ordering schemes $d_{xy} < d_{xz},d_{yz}$. In the orbital scheme the z axis is taken to lie along the O=Os=O axis while the y axis bisects the bipyridine ligands. The relative orbital energies are predicted on the basis of the antibonding character imparted to d_{xz},d_{yz} from dπ(Os)–p(O) mixing and oxo → Os(VI) electron donation. Electronically, the situation is analogous to the d^2 *trans*-dioxo complexes of Re(V) studied spectroscopically by Winkler and Gray, which have $^1A_{1g}(d_{xy})^2$ ground states.[10]

For the C_2 symmetry of the cis complex, simple molecular orbital arguments predict the ordering $d_{xz},d_{yz} < d_{xy}$ and a triplet ground state. The orbital scheme takes the z axis to be perpendicular to the plane of the *cis*-$Os^{VI}(O)_2$ group and assumes greater antibonding character from dπ(Os)–p(O) mixing for the in-plane, d_{xy} orbital. A consequence of the effect of spin–orbit coupling is in mixing d_{xz} and d_{yz}. However, the observed diamagnetism may also be a result of the *cis*-dioxo bond angle deviating from 90°. An analysis of the ratio of the intensities of the symmetric and asymmetric (Os=O) stretching vibrations in the IR region predicts a bond angle of ~130° for the "cis" isomer on the basis of the relation

$$2\theta = 2 \text{ arc cot } (I_{sym}/I_{asym})^{1/2}$$

where 2θ is the O=Os=O bond angle in *cis*-$[(bpy)_2Os^{VI}(O)_2]^{2+}$ and I_{sym} and I_{asym} are the respective integrated intensities of the IR bands.[11] The analysis suggests that the O=Os=O angle may deviate considerably from 90°. The lowering of symmetry would remove the degeneracy of the d_{xz},d_{yz} orbitals and, if the splitting is sufficiently large, could lead to the observed diamagnetic ground state. We have not attempted a detailed analysis of the electronic structure.

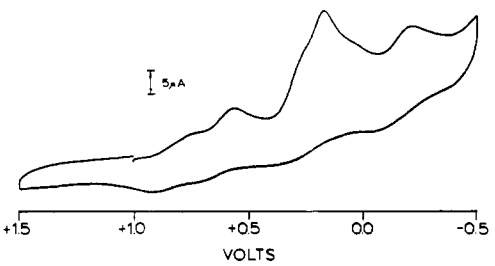

Figure 10. Cyclic voltammogram of ~2 mM *cis*-$[(bpy)_2Os(O)_2]^{2+}$ in CH_3CN/0.1 M tetrabutylammonium hexafluorophosphate (scan rate 100 mV/s).

Oxidation States. The voltammetric studies on *cis*-$[(bpy)_2Os(OH_2)_2]^{2+}$ show that oxidation states II–VI are all accessible within the solvent limits by a series of sequential one-electron oxidations. Potentials for the series of couples at pH 4.0 are shown in the Latimer diagram in Scheme I. The formulation of Os(IV) in Scheme I as *cis*-$[(bpy)_2Os^{IV}(O)(OH_2)]^{2+}$ rather than the proton-equivalent dihydroxy form *cis*-$[(bpy)_2Os^{IV}(OH)_2]^{2+}$ is based on the existence of known Os^{IV}=O and Ru^{IV}=O complexes like *cis*-$[(bpy)_2(py)Ru^{IV}=O]^{2+}$.[1]

Scheme I

$$[b_2Os^{II}(OH_2)_2]^{2+} \xrightarrow{0.04\text{ V}} [b_2Os^{III}(OH_2)(OH)]^{2+} \xrightarrow{0.41\text{ V}} [b_2Os^{IV}(O)(OH_2)]^{2+} \xrightarrow{0.48\text{ V}} [b_2Os^{V}(OH)(O)]^{2+} \xrightarrow{0.67\text{ V}} [b_2Os^{VI}(O)_2]^{2+}$$

(pH 4.0, cis series; vs. SSCE; b is bpy)

A remarkable feature in Scheme I is the appearance of five oxidation states from II to VI without a change in coordination number over a potential range of ~0.6 V. An important contribution to the plethora of oxidation states is the stabilization of the higher oxidation states by proton loss and hydroxo → M and/or oxo → M electronic donation. The importance of proton loss is shown by the potentials for the *cis*-$[(bpy)_2OsCl_2]^{2+/+}$ Os(IV)/Os(III) ($E^{0\prime}$ = 1.51 V vs. SCE in CH_3CN, μ = 0.1 M) and *cis*-$[(bpy)_2OsCl_2]^{+/0}$ Os(III)/Os(II) ($E^{0\prime}$ = –0.04 V) couples.[2a] The large difference in potentials ($\Delta E^{0\prime}$ = 1.56 V) is in marked contrast to the 0.37 V difference between the Os(IV)/Os(III) and Os(III)/Os(II) couples in Scheme I. A second important factor is the role of the solvent, water, as both a proton source and proton acceptor. As shown in Figure 10, in polar organic solvents where no capability exists for facile gain or loss of protons, the electrochemistry is at best ill defined.

The pH dependences of the various couples were inferred from the variations in $E_{1/2}$ values with pH as summarized in the Pourbaix diagram in Figure 5. From the Nernst equation the slopes of the $E_{1/2}$ vs. pH plots depend on the electron–proton contents of the couples as follows: 0 mV/pH unit, $1e^-$; 59 mV/pH unit, $1e^-/1H^+$ or $2e^-/2H^+$; 88 mV/pH unit, $2e^-/3H^+$; 118 mV/pH unit, $1e^-/2H^+$. The sometimes bizarre pH dependences arise from the acid–base properties of the components of the various couples and changes in pK_a values induced by changes in oxidation state. In particular, the series of four breaks in the line for the Os(III)/Os(II) couple reflect the changes in proton content through the series of couples

$$[(bpy)_2Os^{III}(OH_2)_2]^{3+} + e^- \rightarrow [(bpy)_2Os^{II}(OH_2)_2]^{2+}$$

$$[(bpy)_2Os^{III}(OH)(OH_2)]^{2+} + e^- + H^+ \rightarrow [(bpy)_2Os^{II}(OH_2)_2]^{2+}$$

$$[(bpy)_2Os^{III}(OH)_2]^{+} + e^- + 2H^+ \rightarrow [(bpy)_2Os^{II}(OH_2)_2]^{2+}$$

$$[(bpy)_2Os^{III}(OH)_2]^{+} + e^- + H_2O \rightarrow [(bpy)_2Os^{II}(OH)(OH_2)]^{+} + OH^-$$

$$[(bpy)_2Os^{III}(OH)_2]^{+} + e^- \rightarrow [(bpy)_2Os^{II}(OH)_2]$$

(8) Schwarz, W. M.; Shain, I. *J. Phys. Chem.* **1965**, *69*, 30.
(9) Cerney, R. L.; Sullivan, B. P.; Bursey, M. M.; Meyer, T. J. *Anal. Chem.* **1983**, *55*, 1954.
(10) Winkler, J. R.; Gray, H. B. *Inorg. Chem.* **1985**, *24*, 346.
(11) Cotton, F. A.; Wilkinson, G. *Advanced Inorganic Chemistry*, 4th ed.; Wiley: New York, 1980.

Table II. Comparative Summary of Reduction Potentials for Cis and Trans Couples of $[(bpy)_2Os(O)_2]^{2+}$ at Various pH Values (b = bpy, 2,2′-Bipyridine) at 25 °C in H_2O (μ = 0.1 M)

pH	cis couples	$E^{0\prime}$, V	trans couples	$E^{0\prime}$, V
1.0	$[b_2Os^{VI}(O)_2]^{2+}/[b_2Os^{V}(O)(OH)]^{2+}$	0.81	$[b_2Os^{VI}(O)_2]^{2+}/[b_2Os^{III}(OH_2)(OH)]^{2+}$	0.51
	$[b_2Os^{V}(O)(OH)]^{2+}/[b_2Os^{III}(OH_2)_2]^{3+}$	0.64		
	$[b_2Os^{III}(OH_2)_2]^{3+}/[b_2Os^{II}(OH_2)_2]^{2+}$	0.16	$[b_2Os^{III}(OH_2)(OH)]^{2+}/[b_2Os^{II}(OH_2)_2]^{2+}$	−0.03
7.0	$[b_2Os^{VI}(O)_2]^{2+}/[b_2Os^{V}(O)_2]^{+}$	0.57	$[b_2Os^{VI}(O)_2]^{2+}/[b_2Os^{III}(OH)_2]^{+}$	0.25
	$[b_2Os^{V}(O)_2]^{+}/[b_2Os^{III}(OH)_2]^{+}$	0.31		
	$[b_2Os^{III}(OH)_2]^{+}/[b_2Os^{II}(OH_2)_2]^{2+}$	−0.24	$[b_2Os^{III}(OH)_2]^{+}/[b_2Os^{II}(OH_2)_2]^{2+}$	−0.51
10.0	$[b_2Os^{VI}(O)_2]^{2+}/[b_2Os^{V}(O)_2]^{+}$	0.58	$[b_2Os^{VI}(O)_2]^{2+}/[b_2Os^{V}(O)_2]^{+}$	0.21
	$[b_2Os^{V}(O)_2]^{+}/[b_2Os^{III}(OH)_2]^{+}$	0.13	$[b_2Os^{V}(O)_2]^{+}/[b_2Os^{III}(OH)_2]^{+}$	0.03
	$[b_2Os^{III}(OH)_2]^{+}/[b_2Os^{II}(OH_2)(OH)]^{+}$	−0.47	$[b_2Os^{III}(OH)_2]^{+}/[b_2Os^{II}(OH_2)(OH)]^{+}$	−0.75

The breaks arise where they do because pK_a values for *cis*-$[(bpy)_2Os^{III}(OH_2)_2]^{3+}$ fall at ~2 and 5 and at ~8 and ~11 for *cis*-$[(bpy)_2Os^{II}(OH_2)_2]^{2+}$. For the Os(VI)/Os(V) couple there is a single break at pH ~5.5, signaling a change in proton content from

$$cis\text{-}[(bpy)_2Os^{VI}(O)_2]^{2+} + e^- + H^+ \rightarrow cis\text{-}[(bpy)_2Os^{V}(O)(OH)]^{2+}$$

to

$$cis\text{-}[(bpy)_2Os^{VI}(O)_2]^{2+} + e^- \rightarrow cis\text{-}[(bpy)_2Os^{V}(O)_2]^{+}$$

The circumstances with regard to the occasionally "missing" oxidation state, Os(IV), are more complex. Os(IV) exists as a thermodynamically stable oxidation state over the pH range ~2–5, but the potentials for the $1e^-/1H^+$ couples for Os(V)/Os(IV)

$$cis\text{-}[(bpy)_2Os^{V}(O)(OH)]^{2+} + e^- + H^+ \rightarrow cis\text{-}[(bpy)_2Os^{IV}(O)(OH_2)]^{2+}$$

and Os(IV)/Os(III)

$$cis\text{-}[(bpy)_2Os^{IV}(O)(OH_2)]^{2+} + e^- + H^+ \rightarrow cis\text{-}[(bpy)_2Os^{III}(OH)(OH_2)]^{2+}$$

are within ~70 mV of each other. The loss of Os(IV) above pH 5 and below pH 2 is caused by the proximity of the couples. Past pH 5 and the second pK_a value for Os(III), the Os(IV)/Os(III) couple becomes pH independent

$$cis\text{-}[(bpy)_2Os^{IV}(O)(OH_2)]^{2+} + e^- \rightarrow cis\text{-}[(bpy)_2Os^{III}(OH)_2]^{+}$$

and the potential for the Os(IV)/Os(III) couple crosses over and becomes more positive than the potential for the pH-dependent Os(V)/Os(IV) couple

$$cis\text{-}[(bpy)_2Os^{V}(O)(OH)]^{2+} + H^+ + e^- \rightarrow cis\text{-}[(bpy)_2Os^{IV}(O)(OH_2)]^{2+}$$

after a short pH interval. Past pH 6, *Os(IV) is a stronger oxidant than Os(V)* and becomes unstable with respect to self-oxidation/reduction (disproportionation)

$$2\,cis\text{-}[(bpy)_2Os^{IV}(O)(OH_2)]^{2+} \rightarrow cis\text{-}[(bpy)_2Os^{III}(OH)_2]^{+} + cis\text{-}[(bpy)_2Os^{V}(O)(OH)]^{2+} + H^+$$

because of the loss of oxidizing strength for the Os(V)/Os(IV) couple as the pH is increased.

The instability of Os(IV) in more acidic solutions is also triggered by a pK_a at Os(III). At pH ~2 the first pK_a for *cis*-$[(bpy)_2Os(OH_2)_2]^{3+}$ is reached, and the couple becomes

$$cis\text{-}[(bpy)_2Os^{IV}(O)(OH_2)]^{2+} + e^- + 2H^+ \rightarrow cis\text{-}[(bpy)_2Os^{III}(OH_2)_2]^{3+}$$

Below pH 1, the $1e^-/2H^+$ Os(IV)/Os(III) couple crosses over the $1e^-/1H^+$ Os(V)/Os(IV) couple and Os(IV) is, once again, unstable with respect to disproportionation

$$2\,cis\text{-}[(bpy)_2Os^{IV}(O)(OH_2)]^{2+} + H^+ \rightarrow cis\text{-}[(bpy)_2Os^{V}(O)(OH)]^{2+} + cis\text{-}[(bpy)_2Os^{III}(OH_2)_2]^{3+}$$

because the oxidizing strength of Os(IV) is enhanced by the greater proton dependence of the Os(IV)/Os(III) couple. In regions where only the $2e^-$ Os(V)/Os(III) couple is observed, potentials for the component $1\text{-}e^-$ couples are not known. However, it is true that $E^0(IV/III) > E^{0\prime}(V/IV)$ and that the Os(V)/Os(III) potential is the *average* of the two $1\text{-}e^-$ couples.

For the trans series the $E_{1/2}$–pH variations for the Os(III)/Os(II) couple in Figure 7 are understandable on the basis of successive pK_a values of ~0.8 and ~4.3 for *trans*-$[(bpy)_2Os^{III}(H_2O)_2]^{2+}$ and ~8.2 and ~10.1 for *trans*-$[(bpy)_2Os^{II}(OH_2)_2]^{2+}$. The striking feature, of course, is the appearance of the three-electron Os(VI)/Os(III) couple at the expense of oxidation states Os(V) and Os(IV) over a broad pH range. Similar behavior has been previously observed for the close analogue $[(trpy)Os^{VI}(O)_2(OH_2)]^{2+}$.[12] Insight into the missing oxidation states is obtained from the Pourbaix diagram in basic solution where past pH 8, the three-electron wave splits into a pH-independent $1\text{-}e^-$ wave for the Os(VI)/Os(V) couple

$$trans\text{-}[(bpy)_2Os^{VI}(O)_2]^{2+} + e^- \rightarrow trans\text{-}[(bpy)_2Os^{V}(O)_2]^{+}$$

and a $2e^-/2H^+$ wave for the Os(V)/Os(III) couple

$$trans\text{-}[(bpy)_2Os^{V}(O)_2]^{+} + 2e^- + 2H_2O \rightarrow trans\text{-}[(bpy)_2Os^{III}(OH)_2]^{+} + 2OH^-$$

In solutions less basic than pH 8, Os(V) becomes a stronger oxidant than Os(VI), unstable with respect to disproportionation, and only the $3\text{-}e^-$ couple is observed

$$trans\text{-}[(bpy)_2Os^{VI}(O)_2]^{2+} + 3e^- + 2H_2O \rightarrow trans\text{-}[(bpy)_2Os^{III}(OH)_2]^{+} + 2OH^-$$

As for the cis complexes, the appearance of the Os(V)/Os(III) couple at the expense of Os(IV) shows that in basic solution Os(IV) is a stronger oxidant than Os(V) and is unstable with respect to disproportionation. It is an interesting point that at least near pH 8, where the three-electron couple appears, of the three oxidation states Os(VI)/Os(V)/Os(IV), *Os(IV) must be the strongest oxidant thermodynamically*. The order of potentials is $E^{0\prime}(IV/III) > E^{0\prime}(V/IV) > E^{0\prime}(VI/V)$ with $E^0(VI/III)$ the average of the three potentials.

Protonation of an oxo group does not occur for Os(VI) over the pH range studied. This is in contrast to the results of $E_{1/2}$–pH studies on the Os(VI)/Os(III) couple of the related *trans*-dioxo complex *trans*-$[(trpy)Os^{VI}(O)_2OH]^{+}$ (trpy is 2,2′,2″-terpyridine), which have shown pK_a values at 2.4, 6.3, and >14 for $[(trpy)Os^{VI}(O)(OH)(OH_2)]^{3+}$, $[(trpy)Os^{VI}(O)_2(OH_2)]^{2+}$, and $[(trpy)Os^{VI}(O)_2(OH)]^{+}$, respectively.[13]

The data in basic solutions in the Pourbaix diagrams for the cis and trans complexes allow an assessment to be made of the role of stereochemistry at the metal on reduction potentials and on the pattern of stable oxidation states. A comparative summary of reduction potentials for the cis and trans couples at various pH values is presented in Table II. Although there are experimentally meaningful decreases in the potentials of the trans Os(V)/Os(III) and Os(III)/Os(II) couples compared to those of the cis couples, the decrease of ~0.3 V between the two Os(VI)/Os(V) couples is the notable feature in explaining the difference in the pattern of stable oxidation states between cis and trans complexes. The

(12) Pipes, D. W.; Meyer, T. J. *J. Am. Chem. Soc.* **1984**, *106*, 7653.
(13) Pipes, D. W.; Meyer, T. J., submitted for publication.

decrease of 0.3 V is sufficient to lower the Os(VI)/Os(V) couple below the Os(V)/Os(IV) and Os(IV)/Os(III) couples, which explains the 3-e⁻ character observed below pH 8 for *trans*-$[(bpy)_2Os(O)_2]^{2+}$.

A detailed interpretation of the differences in potentials between equivalent cis and trans couples must incorporate both electronic effects and differences in solvation energies. Effects arising from differences in solvation energies should be relatively slight since the charge types on the couples are the same. The smaller value of $E^{0\prime}$ for the trans spin-paired d^5/d^6 M(III)/M(II) couples has precedence in related polypyridine-based couples and has been attributed to electronic effects.[14] Electronic effects no doubt also play an important role in accounting for the considerable stabilization toward the addition of an electron displayed by *trans*-$[(bpy)_2Os(O)_2]^{2+}$ compared to the case of *cis*-$[(bpy)_2Os(O)_2]^{2+}$.

The cis–trans electronic effect is predictable on the basis of simple molecular orbital arguments. For *trans*-$[(bpy)_2Os(O)_2]^{2+}$ the $d\pi$ orbital ordering scheme is $d_{xy} < d_{xz} < d_{yz}$, taking the z axis to lie along the O=Os=O molecular axis. The ground-state configuration for Os(VI) is $(d_{xy})^2$ and for Os(V), $(d_{xy})^2(d_{xz})^1$. The affinity of *trans*-dioxo Os(VI) for an additional electron is expected to be decreased by the considerable antibonding character of d_{xz},d_{yz} arising from d_{xz},d_{yz}(Os)–p(O) mixing.

In terms of a simple MO diagram, the orbital ordering scheme for the cis isomer is $d_{xz},d_{yz} < (d_{xy})$ or, given its diamagnetism $d\pi_1 < d\pi_2 \ll d_{xy}$ with the ground-state electronic configuration, $(d\pi_1)^2$. $d\pi_1$ and $d\pi_2$ are written as if constructed from linear combinations of d_{xz} and d_{yz} including spin–orbit coupling. As long as the $d\pi_1$–$d\pi_2$ energy separation is relatively small, electronic destabilization effects in the reduction of Os(VI) to Os(V), $(d\pi_1)^2 + e^- \rightarrow (d\pi_1)^2(d\pi_2)^1$, will play a lesser role in the cis case compared to trans case.

Both the *cis*- and *trans*-dioxo Os(VI) complexes have an extensive net redox chemistry with a variety of organic and inorganic substrates, and that chemistry is currently under investigation.

Ligand Loss. Ligand loss from *cis*-$[(bpy)_2Os(O)_2]^{2+}$ in water and cis-to-trans isomerization in hot CH_3CN appear to be closely related processes. In water the key is the observation of the intermediate and reactions 2–4. The nature of the intermediate can be inferred from the evidence at hand. The intermediate is the dominant form in solution during the first scan in the continuous cyclic voltammogram in Figure 8c. In that scan an irreversible reduction at −0.03 V is followed by the appearance of reversible waves for the cis Os(V)/Os(III) and Os(VI)/Os(V) couples upon scan reversal. The experiment shows that upon reduction the intermediate is rapidly converted into *cis*-$[(bpy)_2Os^{II}(OH_2)_2]^{2+}$ and demonstrates that at the intermediate stage the bipyridine ligand is yet to be lost.

Perhaps the most reasonable suggestion for the nature of the intermediate is that it contains both a unidentate, ring-opened bpy ligand and the *trans*-dioxo structure favored for d^2 Os(VI) on electronic grounds. The suggested structure has a close analogue in $[(trpy)Os(O)_2OH_2]^{2+}$ (N⌒N⌒N = trpy; N⌒N = bpy) bpy)

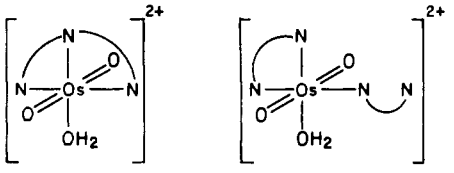

The actual proton composition of the intermediate is, no doubt, pH-dependent. In acidic solution the unbound pyridyl group should be protonated (pK_{a1} = 4.3 for bpy) and perhaps an oxo group as well given the pH dependence of the Os(VI)/Os(III) couple based on $[(trpy)Os(O)_2(OH)]^+$ and the evidence for $[(trpy)Os(O)(OH)(OH_2)]^{3+}$. In sufficiently basic solutions deprotonation of the bound aqua group would give the corresponding hydroxo complex.

(14) Sullivan, B. P.; Meyer, T. J. *Inorg. Chem.* **1982**, *21*, 1037.

Invoking a ring-opened chelate as intermediate in the net ligand loss chemistry is obviously appealing with k_1 in reaction 2 referring to the ring-opening step and k_2 in reaction 3 to ligand loss

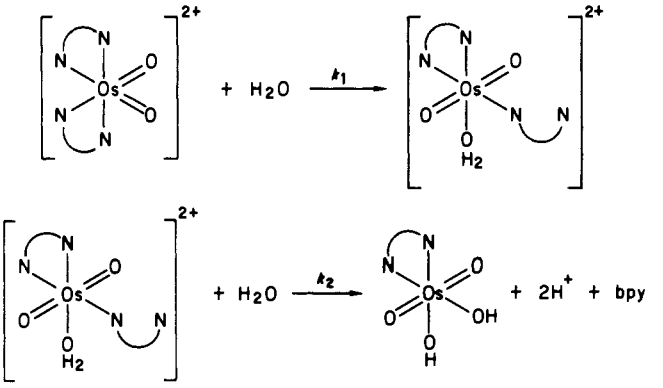

We have made no attempt to treat the pH dependences of k_1 and k_2 in Table I to complex kinetic schemes. One important feature that appears in the data is the obvious pH dependence of k_2, suggesting the existence of a pathway in which ligand loss is induced by protonation of the intermediate at bpy or perhaps at an oxo group.

The reductively induced re-formation of *cis*-$[(bpy)_2Os(OH_2)_2]^{2+}$, reaction 4, is also an expected reaction of a chelate-opened intermediate given the stability of the chelate in oxidation state II and the preference for the cis stereochemistry.

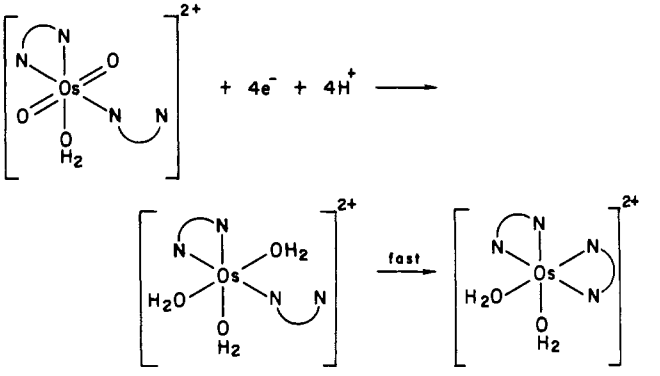

Isomerization. A chelate-ring-opened intermediate may also account for isomerization in acetonitrile but only following an intramolecular rearrangement. In water initial chelate ring opening

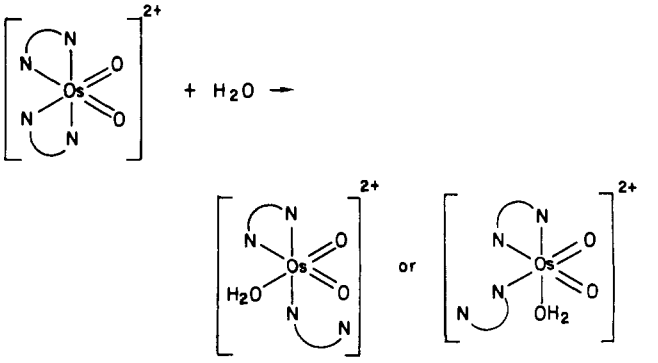

can rapidly lead to cis → trans interconversion by proton transfer from bound aqua to oxo groups

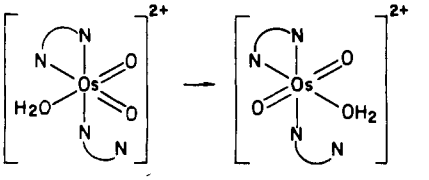

without need for intramolecular rearrangement or further ligand

Scheme II[a]

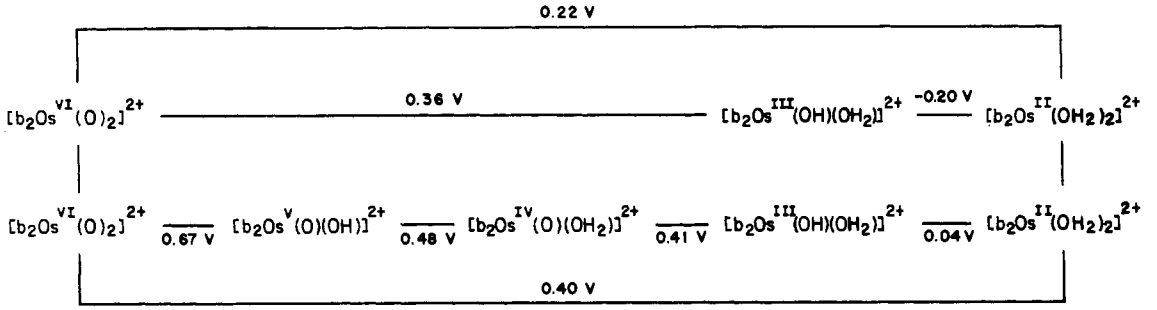

[a] pH 4.0.

loss. In acetonitrile, if the rearrangement is not a concerted intramolecular process

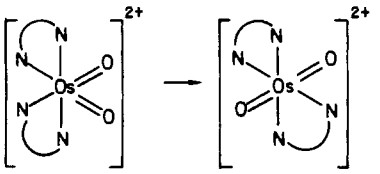

but involves a half-chelate intermediate

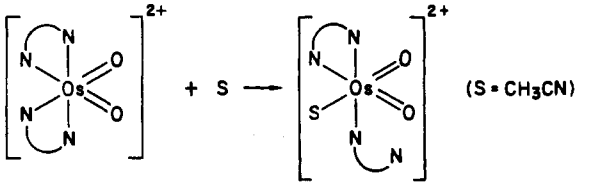

a rearrangement step must occur

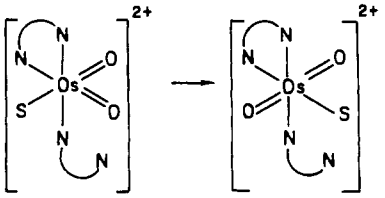

followed by chelate ring closure. Rapid displacement of CH_3CN on Os(VI) is not unexpected given the poor σ-donor character of CH_3CN.

In water the situation is different. On the time scale for ligand loss from *cis*-$[(bpy)_2Os(O)_2]^{2+}$, the *trans*-$[(bpy)_2Os(O)_2]^{2+}$ complex is coordinatively stable. Clearly, in water cis to trans isomerization is not competitive with loss of the half-chelate

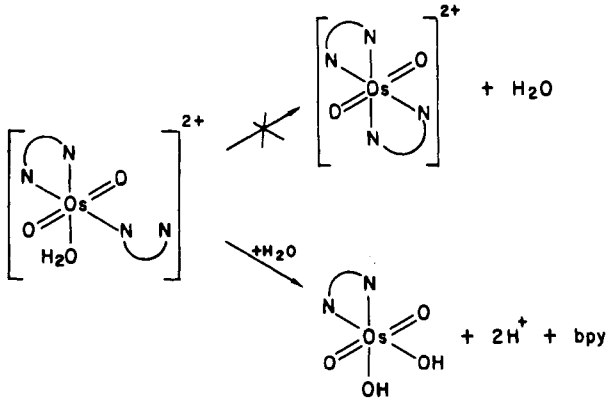

which is a surprise unless H_2O acts as a nucleophile in an associative step in the initial chelate ring opening and the bound aqua group is relatively inert.

The *trans*-$[(bpy)_2Os(O)_2]^{2+}$ complex appears to be thermodynamically more stable than *cis*-$[(bpy)_2Os(O)_2]^{2+}$, at least in hot CH_3CN. The stability of the trans isomer is consistent with the fact that all previously reported monomeric dioxo complexes of Os(VI) also have the trans configuration. The relative stabilities of *cis*- and *trans*-dioxo complexes have been considered on orbital grounds by Atovmyan and Porai-Koshits[15] and Mingos,[16] and the predictions are clear that for the d^2 electronic configuration the *trans*-dioxo configuration is more stable than the *cis*-dioxo configuration.

A second isomerization of note is the conversion of trans to the characteristically more stable cis configuration when Os(VI) is reduced to Os(II)

$$trans\text{-}[(bpy)_2Os^{VI}(O)_2]^{2+} + 4e^- + 4H^+ \rightarrow trans\text{-}[(bpy)_2Os^{II}(OH_2)_2]^{2+} \rightarrow cis\text{-}[(bpy)_2Os^{II}(OH_2)_2]^{2+}$$

On the basis of the redox potentials for the Os(VI)/Os(II) couples at pH 4.0 (vs. SSCE)

$$trans\text{-}[(bpy)_2Os^{VI}(O)_2]^{2+} + 4e^- + 4H^+ \rightarrow trans\text{-}[(bpy)_2Os^{II}(OH_2)_2]^{2+}$$

$$E^{0\prime}(\text{trans}) = 0.22 \text{ V}$$

$$cis\text{-}[(bpy)_2Os^{VI}(O)_2]^{2+} + 4e^- + 4H^+ \rightarrow cis\text{-}[(bpy)_2Os^{II}(OH_2)_2]^{2+}$$

$$E^{0\prime}(\text{cis}) = 0.40 \text{ V}$$

it is possible to obtain a numerical value for the sum of the differences in stability between cis and trans isomers in the two oxidation states

$$4[E^{0\prime}(\text{cis}) - E^{0\prime}(\text{trans})] = \Delta G^{\circ\prime} = [\Delta G_f^{\circ}(\text{cis-II}) - \Delta G_f^{\circ}(\text{trans-II})] - [\Delta G_f^{\circ}(\text{cis-VI}) - \Delta G_f^{\circ}(\text{trans-VI})] = -0.72 \text{ eV} = -16 \text{ kcal/mol}$$

Note the Latimer-type diagram for the cis and trans couples at pH 4.0 in Scheme II. The free energy change calculated is for the reaction

$$cis\text{-}[(bpy)_2Os^{VI}(O)_2]^{2+} + trans\text{-}[(bpy)_2Os^{II}(OH_2)_2]^{2+} \rightarrow cis\text{-}[(bpy)_2Os(OH_2)_2]^{2+} + trans\text{-}[(bpy)_2Os(O)_2]^{2+}$$

$$\Delta G^{\circ} = -0.72 \text{ eV}$$

Although there is no way to apportion the −16 kcal/mol between stabilization of the trans isomer in Os(VI) and that of the cis isomer in Os(II), the magnitude is relatively large. It is especially significant in the context of controlling redox properties. For example, by utilization of an appropriate ligand to constrain the coordination geometry to be cis at the metal, it may be possible in a systematic way to enhance the thermodynamic oxidizing capabilities of Os(VI) and Ru(VI) dioxo systems.

Acknowledgments are made to the National Science Foundation under Grant No. CHE-8304230 for support of this research.

Registry No. *cis*-$[b_2Os(O)_2](ClO_4)_2$, 101980-20-5; *trans*-$[b_2Os(O)_2](ClO_4)_2$, 102045-51-2; $(bpy)_2OsCO_3$, 81831-23-4; *cis*-$[b_2Os(O)(OH)]^{2+}$, 84988-28-3; *cis*-$[b_2Os(OH_2)_2]^{3+}$, 101980-21-6; *cis*-$[b_2Os(OH_2)_2]^{2+}$, 84988-25-0; *cis*-$[b_2Os(O)_2]^{+}$, 101980-22-7; *cis*-$[b_2Os(OH)_2]^{+}$, 101980-23-8; *cis*-$[b_2Os(OH_2)(OH)]^{+}$, 101980-24-9; *trans*-$[b_2Os(OH_2)(OH)]^{2+}$, 102045-52-3; *trans*-$[b_2Os(OH_2)_2]^{2+}$, 102045-53-4; *trans*-$[b_2Os(OH)_2]^{+}$, 102045-54-5; *trans*-$[b_2Os(O)_2]^{+}$, 102045-55-6; *trans*-$[b_2Os(OH_2)(OH)]^{+}$, 102045-56-7.

(15) Atovmyan, L. O.; Porai-Koshits, M. A. *J. Struct. Chem.* (*Engl. Transl.*) **1969**, *10*, 740.
(16) Mingos, D. M. P. *J. Organomet. Chem.* **1979**, *179*, C29.